energies

MDPI

Article

Enhanced Virtual Inertia Controller for Microgrid Applications

Ahmed Sheir and Vijay K. Sood *

Department of Electrical, Computer and Software Engineering, Ontario Tech University, Oshawa, ON L1G 0C5, Canada; ahmed.sheir@ontariotechu.net
* Correspondence: vijay.sood@ontariotechu.ca

Abstract: Unlike Synchronous Generators (SGs), Virtual Synchronous Generators (VSGs) inertia is not fixed once it is manufactured and only has an upper limit defined by its energy storage components. In this paper, a novel Enhanced Virtual Inertia Controller (EVIC) is proposed. The proposed controller alters the VSG inertia coefficient between two limiting levels in response to a grid transient. The key difference between the proposed controller and the variable inertia controller is that the proposed EVIC causes a smooth transition in the inertia coefficient while the variable inertia controller causes a discontinuous jump in it. The proposed EVIC guarantees an adaptive response to grid dynamics, such that a negligible change occurs at small disturbances and a linear and smooth increase occurs at moderate disturbances. For large disturbances, the proposed controller smoothly oscillates the inertia between two saturation levels, which then quickly returns the converter to its steady-state operating point with minimum oscillations. A qualitative study of the performance and stability margin of the proposed controller was conducted using a large signal model (nonlinear model) of VSG connected to a microgrid. The large signal model provided a complete description of the converter's behaviour under large disturbances, which is the area of interest of the proposed controller. It also contained the small-signal dynamics (linear dynamic) within the vicinity of the equilibrium (steady-state) point. Thus, a complete description of the proposed controller dynamics is conveyed to prove its validity and adaptability.

Keywords: VSG; virtual inertia; alternation inertia; microgrid stability; large signal stability; nonlinear controller

check for updates

Citation: Sheir, A.; Sood, V.K. Enhanced Virtual Inertia Controller for Microgrid Applications. *Energies* **2023**, *16*, 7304. https://doi.org/10.3390/en16217304

Academic Editors: Malabika Basu and Sandipan Patra

Received: 13 September 2023
Revised: 24 October 2023
Accepted: 25 October 2023
Published: 27 October 2023

Copyright: © 2023 by the authors. Licensee MDPI, Basel, Switzerland. This article is an open access article distributed under the terms and conditions of the Creative Commons Attribution (CC BY) license (https://creativecommons.org/licenses/by/4.0/).

1. Introduction

The stability of a conventional power system is largely focused on the fundamental characteristics of a Synchronous Generator (SG). By analyzing its output voltage, power and frequency, a distinction can be made between, for instance, different levels of load transients or faults. However, adding more distributed generators deteriorates the grid stability [1,2]. Thus, a Virtual Synchronous Generator (VSG) is introduced to preserve such characteristics while enabling the integration of a variety of renewable energy sources and energy storage systems [3]. The fundamental concept behind VSG control is to add the swing equation of the SG to the converter control loops to modify its output frequency and power angle based on the deviation from a reference power. Thus, the converter can emulate the characteristics of a droop-controlled SG [4–7]. The generic block diagram of such a controller is shown in Figure 1, where the swing equation [8] (Equation (1)) on the right-hand side is obtained by subtracting the converter's real output power P_{out} from the reference power P_{in}. The output is then divided by the inertia coefficient M and is integrated to obtain the frequency deviation $\omega = \omega_i - \omega_r$ (where ω_i is the converter's frequency and ω_r is the rated/reference frequency). The resultant frequency deviation ω is then multiplied by the damping coefficient D to provide negative feedback to damp output power. The converter's power angle is finally calculated by integrating the frequency deviation ω.

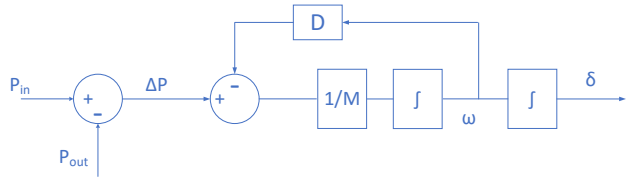


Figure 1. Generic block diagram of the virtual inertia controller.

This approach not only maintains grid stability but can further improve it while guaranteeing proportional load sharing in grid connection and islanding mode of operations [9–17]. In ref. [14], modified virtual synchronous generator control for parallel inverters is introduced. The design of virtual inertia in conjunction with the communication-less control method is proposed to control the active and reactive powers within a small microgrid (MG) accurately. However, the design is carried out based on a linearized model, which has its stability proven under small-signal perturbations. It did not deal with the issue of transient power oscillation or nonlinear region of stability under large signal disturbances.

From a power–frequency point of view, the SG and VSG responses to different kinds of disturbances are proportional to their inertia coefficients based on their swing equations. That is, if the inertia coefficient is relatively low, the rate of change of frequency (RoCoF) within a given MG is higher. On the positive side, it results in a fast response and shorter settling times. Nonetheless, it leads to high frequency and power oscillations and a reduction in stability margins. A higher inertia coefficient results in a sluggish response, which affects the power-sharing among different SGs and hurts the stability. It, however, reduces the power and frequency oscillations to a low level [18]. Fortunately, unlike SGs, the VSGs' inertia is not fixed once it is manufactured and only has an upper limit defined by its energy storage components, such as the dc-link capacitor, ultra-capacitors, batteries, and super inductors; this limits the controller to adjust the inertia coefficient in real time to improve system response and is only bounded by its upper limit.

A new family of inertia controllers has been developed by taking advantage of such properties. These types of controllers were first introduced in [19] and are referred to as alternative inertia, variable inertia, or synthetic inertia. A generic block diagram is shown in Figure 2, where the inertia coefficient is adjusted continuously or discontinuously based on the transient energy in the grid, as shown in the swing equation (Equation (2)). In [19,20], a variable inertia controller discontinuously varied the inertia coefficient using a piece-wise function, in which the inertia coefficient had only two values (maximum and minimum), which were assigned based on the sign of the rate of variation of the power angle and RoCoF (positive or negative). Thus, for any given small variation in either quantity, the inertia coefficient varied by a very large magnitude. Moreover, in the presence of measurement noise, there is no way to know the value of inertia assigned to a given VSG in the MG; this adds more ambiguity to the VSG parameters at any given operating point (even at steady state) and adds complexity to any MG stability analysis.

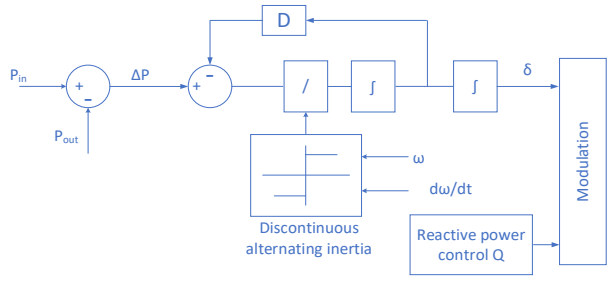


Figure 2. Block diagram of discontinuous alternating virtual inertia controller.

A fuzzy secondary controller (FSC) based virtual inertia was proposed in [13], which utilized the variable inertia concept to improve both voltage and frequency regulation, as well as the dynamic performance of VSG. A system of two parallel converters is used to test the FSC against droop-controlled power converters. Similar work was carried out in [12] but was based on artificial intelligence-based controllers. Although both techniques achieved good results, they relied on complex to-design and to-tune controllers that require a high-performance digital controller with significant computation time. Moreover, the large signal transient and stability margins were not investigated in either technique.

This work proposes a new nonlinear controller that enhances system response and increases stability. The proposed enhanced virtual inertia controller (EVIC) changes the VSG inertia coefficient as a function of the transient energy (disturbance) introduced to the system. It relies on a simple tunable nonlinear equation without any extra sensors, complex algorithms, or prior knowledge of MG configuration or parameters. Thus, it can further improve the grid stability margins and reduce power oscillations. Furthermore, similar to [13,21], the proposed controller provides adaptive alternating inertial dynamics in proportion to the applied disturbances, which is further explained in Section 3. The contribution of this work can be summarized as follows:

- Proposing a new enhanced virtual inertia controller based on a simple nonlinear function with easy-to-tune parameters. The proposed controller provides adaptive behaviour, which makes it robust against uncertainty and measurement noise while being able to dampen VSG output power and frequency oscillations quickly;
- Studying the converter's large signal response and stability using a graphical approach to demonstrate its positive impact on the grid region of stability;
- Successfully implementing the proposed controller and testing it against different levels of disturbances.

The rest of this journal paper is arranged as follows: Section 2 provides a background on the alternating inertia controller concept. The proposed EVIC and its design parameters are explained in Section 3, while its large signal response is dealt with in Section 4. Simulation results are discussed in Section 5. And finally, conclusions are provided in Section 6.

2. Concept of Alternating Inertia

The value of the virtual inertia in a given VSG is varied based on the rate of change of its power angle $d\delta/dt$ and its acceleration $d^2\delta/dt^2$. That is, if they are going in the same direction, i.e., they have the same signs, this means the VSG is going in the right direction, and its inertia is switched to a higher value to prevent oscillation. On the other hand, if their signs are different, this means that the VSG is going in the wrong direction (away from the steady-state point); hence, the inertia is switched to a lower value to shorten such overshoot/undershoot periods. The block diagram of such a technique is shown in Figure 2. It utilizes the same block diagram of the conventional virtual inertia controller shown in Figure 1, but there is one major difference. That is, instead of dividing by constant inertia coefficient M, it is divided by a discontinuous piece-wise function $M\left(\omega, \frac{d\omega}{dt}\right)$, which has two saturation levels: M_{min} and M_{max}. As will be explained shortly, this function alters the converter's inertia coefficient based on its accelerating/deaccelerating power based on its two-feedback frequency deviation ω and RoCoF $\frac{d\omega}{dt}$. The rest of the block diagram remains unchanged and operates in the same way.

This concept is further explained as follows: Suppose a VSG, in a single source VSG microgrid, operates at the steady state power angle δ^{s1}, as shown in Figure 3. If the load power increases, the steady-state power angle moves from δ^{s1} to δ^{s2} to satisfy the load demand. The transient from δ^{s1} to δ^{s2} is oscillatory due to the existence of complex eigenvalues. On the power curve, this means that the operating point moves from point a to point b, which results in a positive rate of change of frequency (RoCoF) $\frac{d^2\delta}{dt^2}$, or in other words, acceleration, while the rate of change in power angle is positive as well $\frac{d\delta}{dt}$. Once it

passes point b towards point c, the rate of change in frequency (RoCoF) becomes negative, while the rate of change in power angle is still positive, which means deceleration. On the other hand, the rate of change in power angle is still positive.

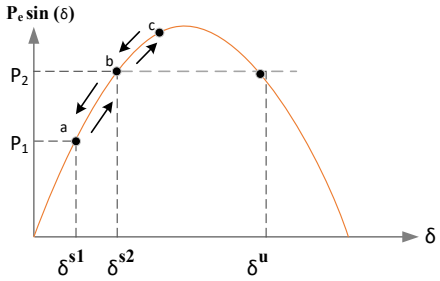


Figure 3. VSG power angle transient oscillation.

The same behaviour is repeated in the opposite direction. That is, the system accelerates once it starts to move back from point c to point b and decelerates after crossing point b toward point a. This cycle is repeated until the VSG settles on the new operating point b at the new power angle δ^{s2}. Such an oscillation is reflected mainly in the output power, as the input power here is virtual. It also greatly impacts the stability of MGs, especially the ones with multiple VSGs, as such oscillations can be amplified and result in loss of synchronism [8].

It can be seen from the typical swing Equation (1) for the preceding scenario that the acceleration direction is the desirable one, as it means that the inverter is moving toward the steady-state point. While in deceleration, it moves away from it. Therefore, it is desirable to shorten the deceleration periods and magnitude as much as possible in favour of the acceleration ones.

$$M\frac{d^2\delta}{dt^2} + D\frac{d\delta}{dt} = (P_m - P_e\sin(\delta)) \tag{1}$$

To achieve such an objective, the inertia coefficient M is altered as a function of the RoCoF and power angle. That is, during acceleration periods, the inertia is set to its normal (maximum) value, giving the MG time to detect the RoCoF and adjust its parameters (e.g., secondary and tertiary control parameters, protection relies on, etc.). During the deceleration periods, the inertia M is set to a lower value, which reduces the magnitude and the time constant of the VSG. It is worth mentioning that this is only possible in VSG-controlled inverters, as their inertia is just a virtual quantity M with only an upper limit tied to a physical quantity M_{max}.

In the literature, the inertia coefficient M is alternated discontinuously between two values: M_{max} during acceleration and M_{min} during deceleration. Equation (2) formulizes this technique as follows [19,20,22–24]:

$$M(\omega, \frac{d\omega}{dt}) = \begin{cases} M_{max} & \frac{d\delta}{dt} \times \frac{d^2\delta}{dt^2} > 0 \quad (acceleration) \\ M_{min} & \frac{d\delta}{dt} \times \frac{d^2\delta}{dt^2} < 0 \quad (deceleration) \end{cases} \tag{2}$$

Although this technique has proven to be effective, it suffers from some drawbacks due to its discontinuous nature. The VSG inertia changes abruptly during a transition between the two levels, no matter how small the disturbance is, which does not guarantee system stability. In other words, for small disturbances, such as a small load change, the VSG inertia alternates between the highest and lowest values (defined in Equation (2)), which is the exact same response in the case of large disturbances. Moreover, during steady-state operation, inertia chattering is noticed because of negligible variations in the frequency and power angle or measurement noises.

From a stability point of view, it is difficult to study or prove the stability of an MG under alternative virtual inertia control. It is impossible to use linear analysis tools such as Nyquist or root-locus, as they require linearization around one operating point, i.e., one inertia value. Regardless, studying the system under the two values of inertia only shows the stability range between these two values without providing any qualitative or quantitative insights into system performance. More importantly, due to linearization, such linear analysis does not guarantee an accurate stability estimate under large disturbances, i.e., far from the linearized segment. Finally, such a study, assuming it is satisfactory, cannot be extended to an MG formed with multiple VSGs, as there is no way to instantaneously correlate the inertia coefficient of each VSG with respect to the others or the applied disturbance.

Although nonlinear analysis overcomes the limitations imposed by linearization, studying a system with switching behaviour, such as jumping discontinuously between two different states, requires special treatment and theories which cannot be easily generalized or extended. It is worth mentioning here that Lyapunov and Lyapunov-like stability analysis tools are limited to smooth and continuously differentiable systems [25].

It can be seen from the preceding discussion that a new control technique is needed to overcome the drawbacks of the conventional alternating inertia technique without compromising its appreciated merits.

3. Proposed Enhanced Virtual Inertia Controller (EVIC)

The proposed enhanced virtual inertia controller (EVIC) is based on an alternating inertia technique, which is shown in Figure 2 and formulated in Equation (2). That is, the inertia coefficient alternates between two levels in response to a grid transient. The key difference is that the proposed EVIC causes a smooth transition in the inertia coefficient, while an alternating inertia controller causes a discontinuous jump in it.

In the proposed controller, inertia Equation (2) is replaced by the proposed Equation (3) as follows:

$$M(\Delta P, \omega) = \mathrm{M}_{nom} + \frac{\Delta M}{2}\tanh(a\Delta P\omega) \tag{3}$$

where:

M_{nom} is the inertia nominal value at the steady state;

ΔM is the difference between the minimum and maximum allowable variation in M, i.e., $\Delta M = M_{max} - M_{min}$;

a is the slope of inertia variation in the linear region;

ΔP is the difference between the virtual input mechanical power and output electrical power of a VSG;

ω is VSG frequency variation, which equals the rate of variation of VSG power angle $d\delta/dt$ with respect to the reference frame.

An understanding of some of the properties of the hyperbolic function $\tanh(.)$ is needed to understand the origin and behaviour of the proposed controller. Typical $\tanh(x)$ curves are plotted in Figure 4. At small values of $|x|$, $\tanh(x)$ is almost a linear unity gain over the domain $|x| < 1$. Beyond that, $\tanh(x)$ acts as an ideal saturation function with a peak range of one $|\tanh(x)| = 1 \forall |x| \geq 1$. It is obvious then that $\tanh(x)$ provides a smooth transition between its linear region and saturation and conveniently between its upper and lower saturation limits. Moreover, the linear gain region can be adjusted with the coefficient a $[\tanh(a\ x)]$ to be sharper or more relaxed, as shown in Equation (4). Saturation levels can also be scaled with the coefficient b $[b\tanh(a\ x)]$. Finally, a bias level c can be added to maintain the variation within the positive domain. Thus, based on these parameters, the function is rewritten as follows:

$$z(x) = c + b\tanh(a\ x) \tag{4}$$

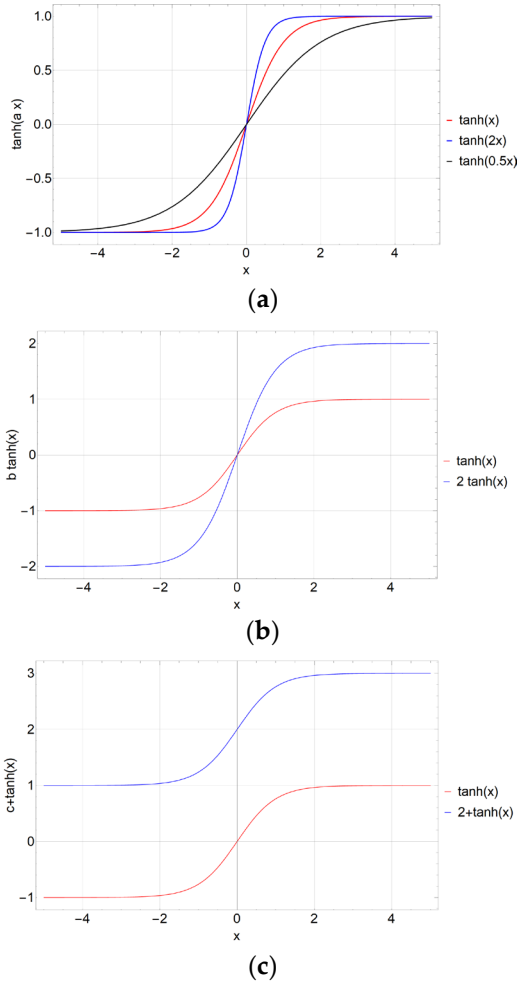


Figure 4. Plot of different $\tanh(x)$ based functions; (**a**) $\tanh(ax)$ at $a = 0.5, 1,$ and 2; (**b**) $b\tanh(x)$ at $b = 1,$ and 2; and (**c**) $c + \tanh(x)$ at $c = 0,$ and 2.

The proposed EVIC benefits from these properties in controlling the inertia coefficient in a VSG. In fact, Equation (4) is identical to the controller Equation (3).

$$z(x) = M(\Delta P, \omega) \tag{5}$$

where the bias level is inertia nominal value $c = \mathrm{M}_{nom}$.

The saturation levels are the minimum and maximum variations in inertia and are expressed as:

$$b = \frac{\Delta M}{2} = (M_{max} - M_{min})/2 \tag{6}$$

The slope of the inertia varies in the linear region a, which is set based on the design preference.

Finally, x is the product of the power mismatch and frequency deviation $x = \Delta P\omega$. The proposed EVIC controller is shown in Figure 5 and can be explained as follows. In a steady state, both virtual input power and electrical output power are equal; hence, $\Delta P = 0$ p.u. Also, VSG is expected to follow its reference frequency with an appropriate constant power angle δ; hence, $\omega = 0$ p.u. Therefore, EVIC Equation (3) becomes (8), and the converter's inertia equals to its nominal value M_{nom} as follows:

$$M(\Delta P, \omega) = \mathrm{M}_{nom} + \frac{\Delta M}{2}\tanh(0) \tag{7}$$

$$M(\Delta P, \omega) = \mathrm{M}_{nom} \tag{8}$$

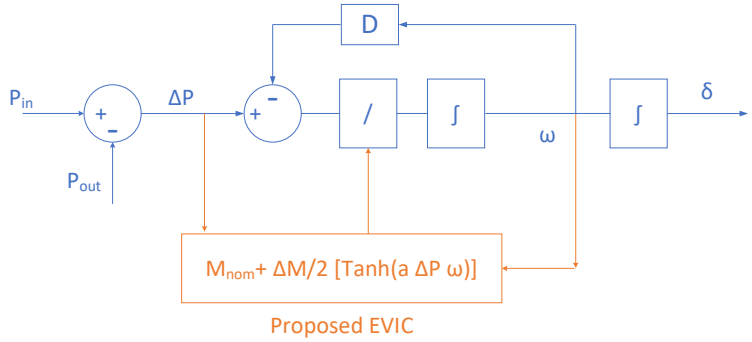


Figure 5. Proposed controller EVIC block diagram.

During a transient state, for example, in the case of a load transient, a mismatch between the virtual mechanical input power and the output electrical power occurs, which causes a positive (acceleration) or negative (deceleration) RoCoF $\left(\frac{d^2\delta}{dt^2} \propto \Delta P\right)$, and a deviation from the reference frequency $\omega = \omega_i - \omega_r$. Therefore, the inputs of the hyperbola function $\tanh(\cdot)$ are no longer zero, and, hence, the converter's inertia varies accordingly, based on Equation (3). However, unlike alternating inertia controller, the variation in inertia does not pulsate between two saturation levels M_{max} and M_{min} despite the magnitude of the transient or disturbance.

The variation in inertia caused by the proposed EVIC is proportional to the magnitude of applied disturbance (e.g., load transient) and how far the VSG converter is from its equilibrium point (operating point at steady state). That is, for a given slope a in Equation (3), for a small load transient, the product of ΔP and ω is small, and, hence, the change in VSG inertia $M(\Delta P, \omega)$ is minimal and can be negligible $M(\Delta P, \omega) \cong \mathrm{M}_{nom}$; this is very useful in a linear study and analysis, where the variation in the converter's states must be practically small. In other words, under linearization, the proposed EVIC can be treated essentially as constant inertia without any practical mismatch between the actual implementation and the linearized model. Such an assumption would not be true in a conventional alternating inertia controller. Moreover, for higher disturbance magnitudes, the proposed EVIC linearly changes the converter's inertia by virtue of its linear region, as explained earlier and shown in Figure 6.

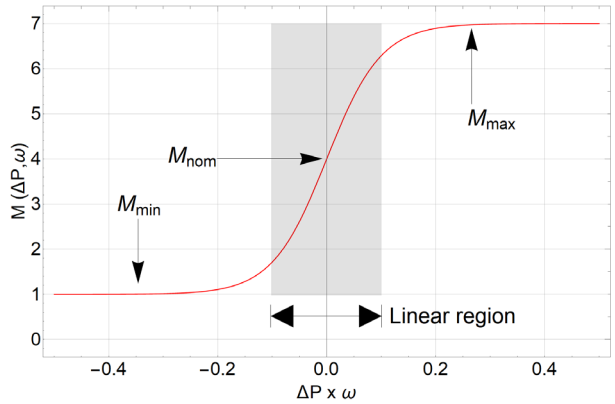


Figure 6. Example of inertia variation using proposed EVIC nominal 4 p.u., minimum 1 p.u., and maximum 7 p.u.

During a disturbance, such as a load transient, the VSG controller is slowly adjusted till its virtual mechanical input power matches its electrical output power based on its droop gain k_p. This results in a gradual reduction in ΔP and ω. In response, EVIC gradually

varies VSG inertia in the same manner towards its nominal value, forcing the converter to its steady state.

Thus, the proposed EVIC guarantees adaptive behaviours as follows:

- For small disturbances (small ΔP and ω), the controller's gain is very small and can be negligible, which eases the linear treatment of the VSG and the microgrid it is connected to;
- For average disturbances, the controller's gain increases linearly with slope a, which varies VSG inertia smoothly around its nominal value between a lower value and a high value (not the maximum and minimum), which quickly damps out the oscillation in power and frequency caused by the disturbance;
- For large disturbances (large signal transient), EVIC oscillates the inertia between its saturation values (M_{max} and M_{min}) causing the converter to quickly return to its steady-state operating point with minimum oscillation in its power and frequency. Moreover, as will be shown next, the closer the converter is to its steady-state operating point, the lower the magnitude of the oscillation in its inertia.

4. Large Signal Dynamics of EVIC

A qualitative study of the performance and stability margin of the proposed controller was conducted using a large signal model (nonlinear model) of VSG connected to an MG, as shown in Figure 7. As opposed to a small-signal model (linearized model), the large signal model provides a complete description of a converter's behaviour under large signal disturbances, which is the area of interest of the proposed controller. It also contains the small-signal dynamics (linear dynamic) within the vicinity of the equilibrium (steady-state) point. Thus, by studying large signal dynamics, a complete description of proposed controller dynamics is conveyed to prove its validity and adaptability.

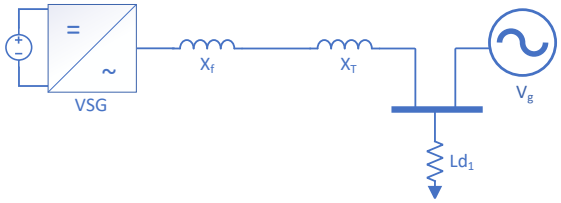


Figure 7. VSG connected to the microgrid.

The large signal model (without EVIC) of a microgrid is shown in Figure 1:

$$\dot{\delta} = \omega$$
$$\dot{\omega} = \frac{1}{M}(P_m - P_e Sin(\delta) - D\omega) \quad (9)$$

where:

δ is VSG's power angle in rad with respect to the grid power angle;
ω is VSG's frequency deviation from the grid power angle ω_g;
P_m is VSG's virtual mechanical input power;
P_e is VSG's rated electrical output power;
D is VSG's damping coefficient;
M is VSG's inertia coefficient.

Based on Equation (3), the EVIC-controlled VSG large signal model is as follows:

$$\dot{\delta} = \omega$$
$$\dot{\omega} = \frac{1}{\mathrm{M}_{nom} + \frac{\Delta M}{2}\tanh(a\Delta P\omega)}(P_m - P_e Sin(\delta) - D\omega) \quad (10)$$

Large signal dynamics of both models formulated in Equations (9) and (10) are visualized by plotting their $\dot{\delta} - \dot{\omega}$ vector field in Figure 8 using the parameters in Table 1. Several integral solutions are plotted starting from different initial points by following the succession vectors field in positive time ($t > 0$). Each curve in Figure 8 shows how the power angle and frequency of VSG change with respect to each other and move either toward the stable equilibrium point or away from it.

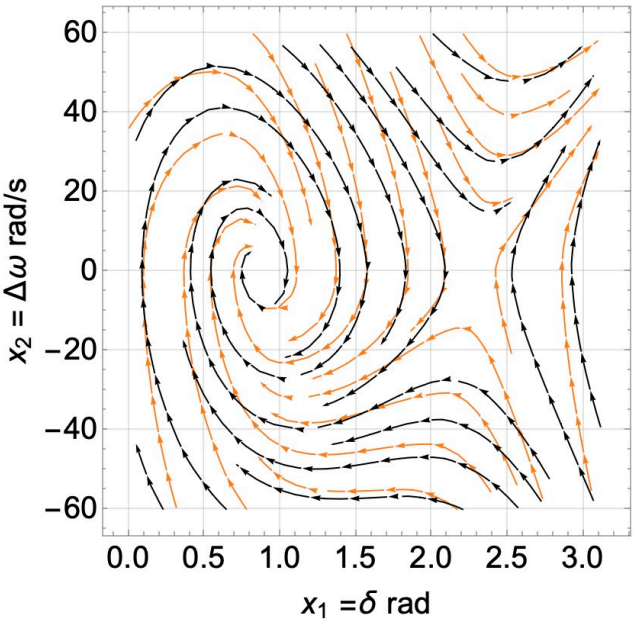


Figure 8. Vector field and integral solution of VSG converter. The black curves are for the conventional inertia controller, and the orange curves are for the proposed EVIC.

Table 1. VSG parameters.

Parameter	Value
Virtual input reference power P_m	0.6 p.u.
Base power S	3.125 MVA
Power angle at steady state δ	0.203 rad
Grid power angle δ_g	0 rad
Line impedance x_g	0.43 p.u.
Grid line voltage v_g	2.4 kV
Active power droop coefficient K_p	0.03
Reactive power droop coefficient K_q	0.03
Damping constant D	1 p.u.
Inertial constant M_{nom} normalized	10 s
Inertial constant M_{min} normalized	5 s
Inertial constant M_{max} normalized	15 s

The black curves in Figure 8 correspond to a VSG with a conventional virtual inertia controller, while the orange curves are for the proposed EVIC. It is worth mentioning that conventional alternating inertia control, represented by Equation (2), is not easy to represent due to its discontinuous nature. Hence, this shows the advantage of the proposed controller in terms of ease of applying all nonlinear analysis tools with no special treatment, compared with conventional alternating inertia.

The converter's behaviour, starting from three different initial conditions, is discussed to demonstrate the advantages of the proposed EVIC over a conventional inertia controller. It is assumed that the VSG converter is subjected to a disturbance that causes it to move away from its equilibrium point to one of these initial conditions. Thus, the following

discussion is related to the converter's recovery from each one of those initial conditions back to its equilibrium point.

The first case is when the converter starts from an initial point far away from the equilibrium point, but it eventually leads to it using both types of controllers. An example of such a case is the initial point ($\delta = 1$ rad, $\omega = 1$ rad/s). The converter's trajectories using the proposed EVIC (in red) and conventional inertia controller (in blue) are plotted on a zoomed area of Figures 8 and 9.

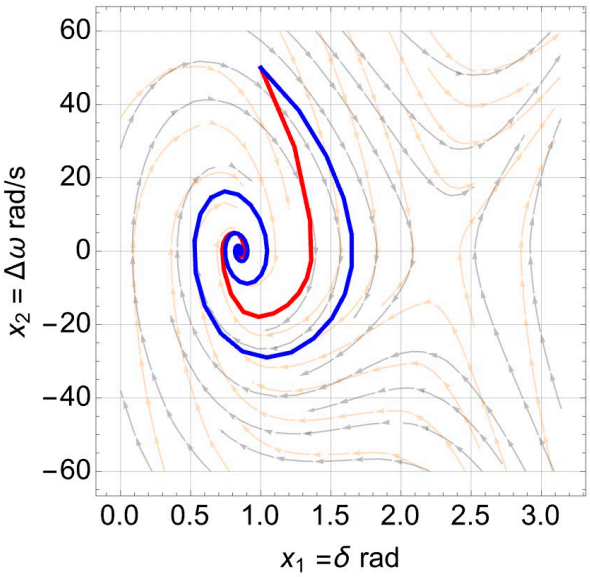


Figure 9. VSG trajectories and dynamics in the first case. The initial point is ($\delta = 1$ rad, $\omega = 50$ rad/s). The conventional inertia controller trajectory is in blue, and the proposed EVIC is in red.

Starting from the same point, the trajectory of a conventional inertia controller (blue in Figure 9) takes a longer path to reach the VSG's equilibrium point, which means it has a longer settling time. Moreover, it has more spiral rotations before reaching the equilibrium point, which translates into more oscillations in the converter's frequency deviation and power angle and, thus, more power oscillations and an increase in losses. On the other hand, the proposed EVIC takes a much shorter path toward the equilibrium point with fewer spiral rotations and, hence, much fewer oscillations; this proves the advantage of the proposed EVIC in bringing the converter very quickly to steady-state after being subjected to a large disturbance or load transient, with minimal oscillation and losses. This is due to its property of smoothly alternating its inertia, based on the profile shown in Figure 6, between its saturation levels away from the equilibrium point and linearly when it is closer to it.

The resultant variation in inertia is shown in Figure 10 for the same aforementioned test conditions. It clearly shows the expected behaviour of the proposed controller. At the start, the VSG converter was far from its equilibrium point; thus, EVIC started with the minimum value of the inertia in Table 1 to quickly bring the converter back to its equilibrium point (acceleration). The closer the converter is to its equilibrium point (shown by its trajectory), the higher its inertia (decelerations) until it reaches its maximum value, as stated in Table 1; this is performed for a few cycles and depends on the severity of the applied disturbances. However, it is still much better than using a conventional inertia controller. At a steady state, the transient amplitude decayed to very low values close to the equilibrium point. Thus, the proposed controller changes the inertia to be almost equal to its nominal value or equal to it at a steady state. Another advantage is that converter inertia is known at any time and instant and can be easily calculated and simulated, unlike the conventional alternating inertia methods, where there is uncertainty and ambiguity in its exact value due to constant variation of virtual inertia, even at a steady state. The

same qualitative results can be observed by choosing any initial point far away from the equilibrium point and following the system's vector field or the set of integral solutions, as shown in Figure 9.

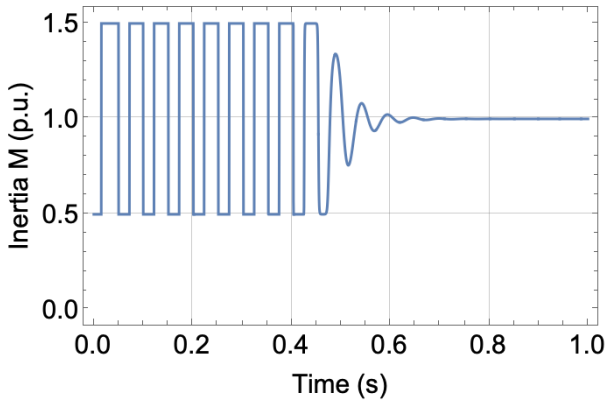


Figure 10. Alternating inertia profile of the proposed EVIC in the first case.

In the second case, the VSG converter starts from an initial point within the unstable region of the conventional inertia controller ($\delta = 1.4$ rad, $\omega = 60$ rad/s). As expected, its trajectory in Figure 11 (shown in blue) does not return to its designated equilibrium point. It follows the vector field and closest integral solutions and moves away from the stable region affected by the unstable eigenvector of the saddle point. In other words, the converter's power angle moves to the unstable quadrant of the swing equation curve. By contrast, the proposed EVIC can bring the trajectory back to the designated equilibrium point, as shown in Figure 8 (shown in red). EVIC inertia profile, shown in Figure 12, is like the one discussed in the first case above.

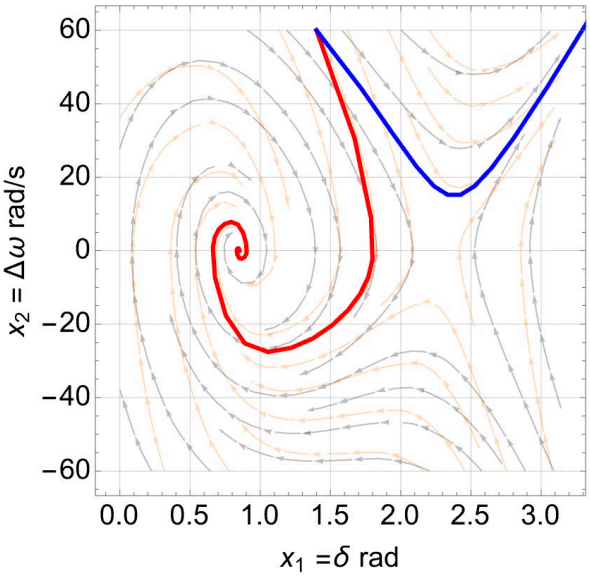


Figure 11. VSG trajectories and dynamics in the second case. The initial point is ($\delta = 1.4$ rad, $\omega = 60$ rad/s). The conventional inertia controller trajectory is in blue, and the proposed EVIC is in red.

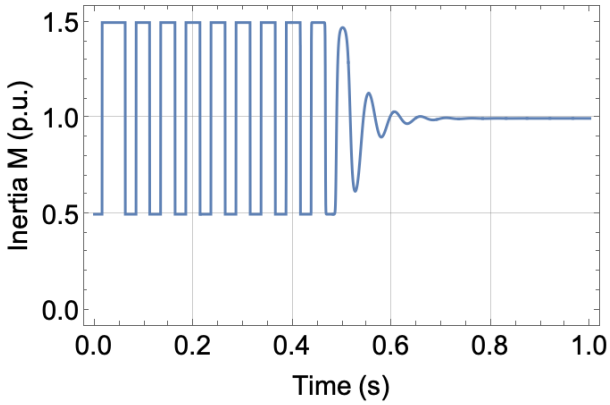


Figure 12. Alternating inertia profile of the proposed EVIC in the second case.

The initial conditions in this case are closer to the first case, and the system exhibits similar dynamics as observed by integral solutions (shown in orange lines). The only difference is a slight increase in the upper transient inertia value, which is within the controller design. This test shows that the proposed EVIC helps reduce oscillation, power loss, and settling time. It also increases the converter's stability region (area of attraction) beyond conventional inertia controllers while maintaining the desired inertial characteristics.

In the third case, the initial point is chosen to be close to the equilibrium point ($\delta = 0.84$ rad, $\omega = 1$ rad/s). As can be seen from the corresponding trajectories (Figure 13) within the vicinity of the equilibrium point, both the proposed EVIC and the conventional inertia controller act almost identically; this demonstrates the advantage of the proposed controller (EVIC) as it does not affect the converter's linear behaviour (i.e., eigenvalues and eigenvectors). This is better shown with the help of Figure 14, which shows a small variation around the nominal inertia coefficient value M_{nom} (stated in Table 1). Hence, it can be assumed to be constant in linearization; this means that all linearized models, analyses, and results are valid under the proposed controller, saving time and effort that would have to be used to build other linear models and study their stability boundaries.

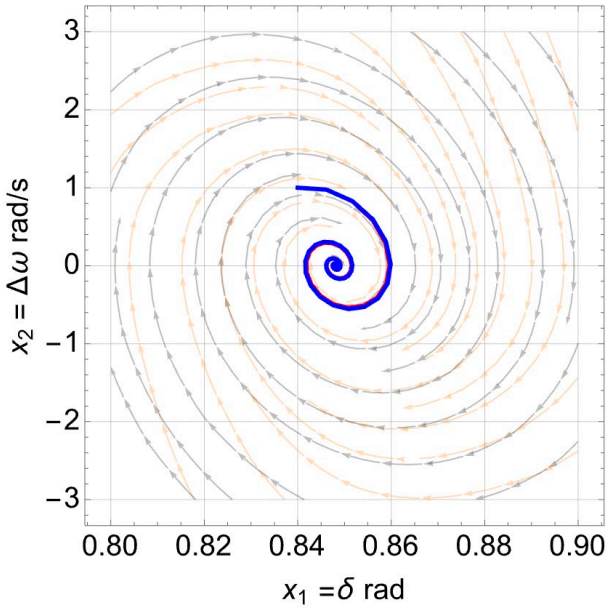


Figure 13. VSG trajectories and dynamics in the third case. The initial point is ($\delta = 0.84$ rad, $\omega = 1$ rad/s). The conventional inertia controller is in blue, and the proposed EVIC is in red.

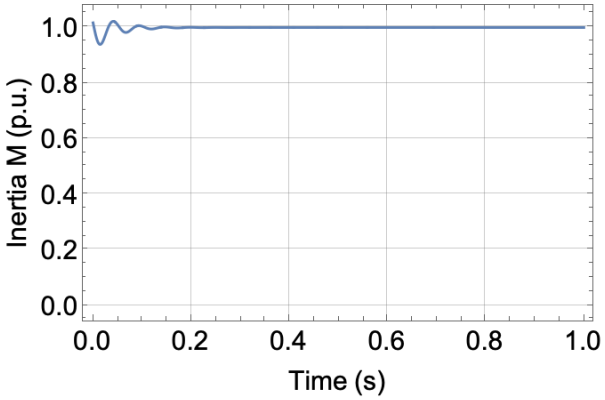


Figure 14. Alternating inertia profile of the proposed EVIC in the third case.

Such behaviour shown in these three cases combined (and summarized in Figure 15) is unique to the proposed controller (EVIC) compared with other types of inertial controllers, such as conventional inertia, alternative discontinuous inertia, and droop control-based inertia emulators. Moreover, the proposed controller does not require any additional measurements, sensors, complicated adaptive algorithms or artificial intelligence [21]. On the contrary, it is easy to implement and does not add any complexity to linear analysis and control while adding more robustness to VSG converters and widening their regions of stability.

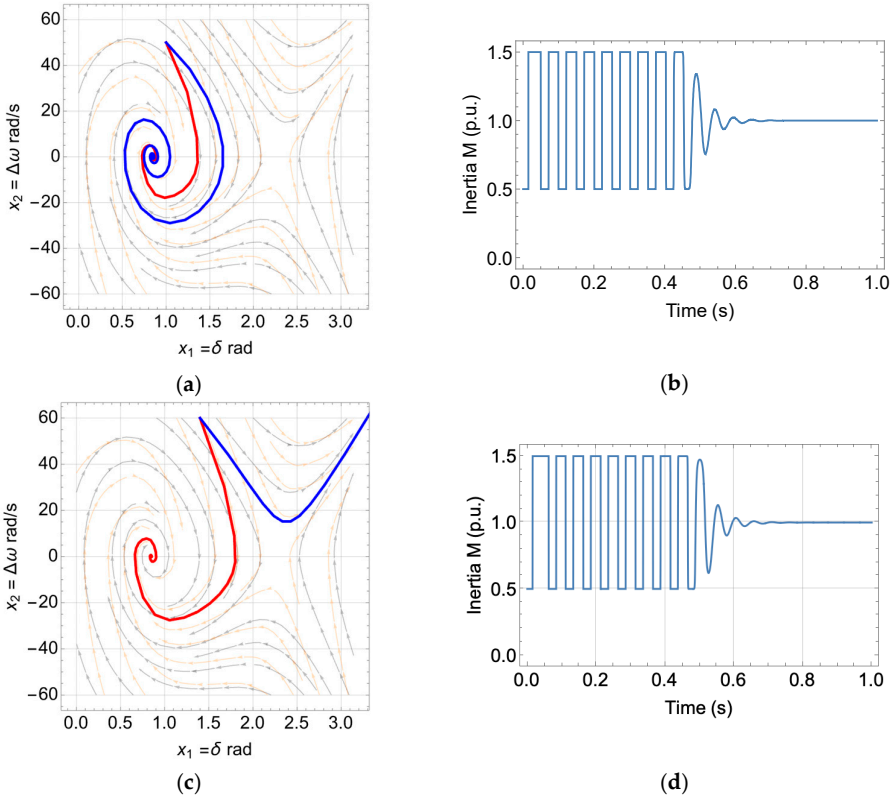


Figure 15. *Cont.*

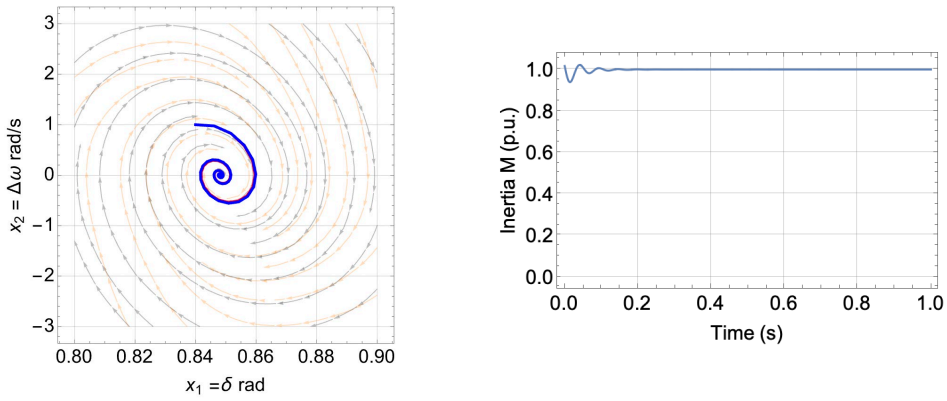


Figure 15. Summary of VSG dynamics in all cases. (**a**) VSG trajectories and dynamics in the first case. The initial point is ($\delta = 1$ rad, $\omega = 50$ rad/s). The conventional inertia controller trajectory is in blue, and the proposed EVIC is in red. (**b**) Alternating inertia profile of the proposed EVIC in the first case. (**c**) VSG trajectories and dynamics in the second case. The initial point is ($\delta = 1.4$ rad, $\omega = 60$ rad/s). The conventional inertia controller trajectory is in blue, and the proposed EVIC is in red. (**d**) Alternating inertia profile of the proposed EVIC in the second case. (**e**) VSG trajectories and dynamics in the third case. The initial point is ($\delta = 0.84$ rad, $\omega = 1$ rad/s). The conventional inertia controller trajectory is in blue, and the proposed EVIC is in red. (**f**) Alternating inertia profile of the proposed EVIC in the third case.

5. Results

A simulation of the proposed controller was conducted to verify its performance using the Matlab/Simulink model. A VSG was connected to an infinite bus using a transformer and a double-circuit transmission line, as shown in Figure 16. The per unit voltage of the infinite bus was set to 1 p.u., while the terminal per unit voltage of the VSG was set to 1.05 p.u. The per unit reactance of the converter's output filter was j0.2 p.u., the transformer reactance was j0.1 p.u., and the reactance of each transmission line was j0.4 p.u. The VSG inertia coefficient was M = $\frac{10}{377}$. The VSG reference power was 0.8 p.u. The base voltage was 13.8 kV, and the base power was 100 MVA. The single-line diagram of the system is shown in Figure 17, and the parameters are listed in Table 2.

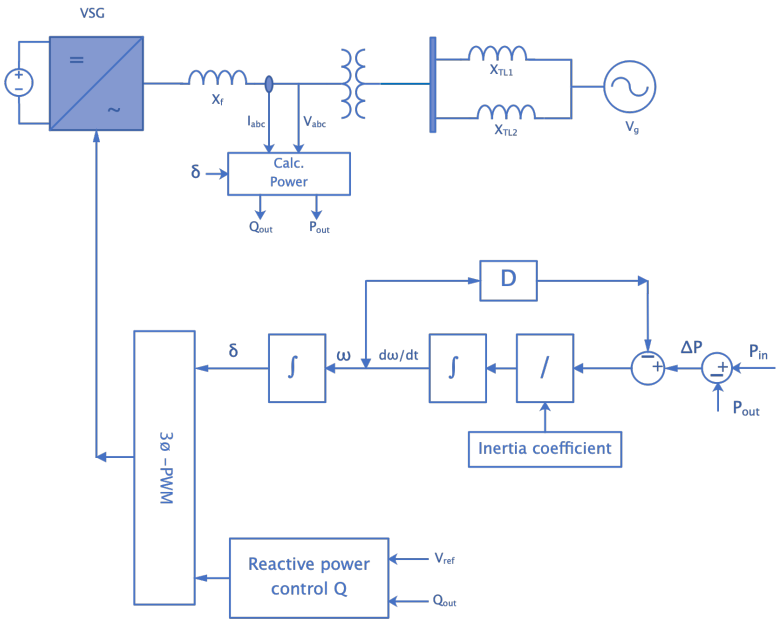


Figure 16. The VSG system was connected to an infinite bus.

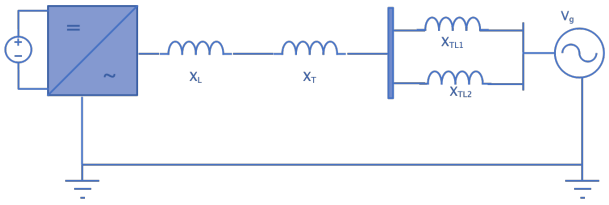


Figure 17. System single-line diagram.

Table 2. VSG simulation parameters.

Parameter	Value
Virtual input reference power P_m	0.8 p.u.
Base power S	100 MVA
Grid line voltage v_g	13.8 kV
Power angle at steady state δ	0.3908 rad
Grid power angle δ_g	0 rad
Total Line impedance	j0.5 p.u.
Infinite bus voltage v_g	1 p.u.
VSG voltage v_g	1.05 p.u.
Damping constant D	0.1
Inertial constant M_{nom} normalized	5 s
Inertial constant M_{min} normalized	2.5 s
Inertial constant M_{max} normalized	7.5 s

The system model under a conventional virtual inertia controller is given by:

$$\dot{\delta} = \omega$$

$$\dot{\omega} = \frac{377}{10}(0.8 - 2.10\ Sin(\delta) - 0.1\omega) \tag{11}$$

Also, the system model under EVIC and the system model is given by:

$$\dot{\delta} = \omega$$

$$\dot{\omega} = \frac{377}{10 + 5\tanh(100\ \Delta P\ \omega)}(0.8 - 2.10\ Sin(\delta) - 0.1\omega) \tag{12}$$

The adaptive performance of the proposed controller was evaluated here using the three cases mentioned in the previous section. In every case, the exact network was simulated twice, once with the conventional inertia controller and the other with the proposed EVIC controller, while keeping all other parameters unchanged.

In the first case, the converter was connected to the infinite bus, and its reference power was set to 0.8 p.u. The initial power angle was $\delta_o = 0$ rad, and the frequency deviation from infinite bus frequency was $\omega_o = 10$ rad/s; this demonstrates the case where the VSG is subjected to a large load disturbance. The results shown in Figure 18 prove the validity and superiority of the proposed controller. Compared with the conventional controller, the overshoot/undershoot of the power angle was reduced by 30%, while the oscillation and transient time were reduced by more than 50% from 2.5 s using a conventional controller to 1 s using the proposed EVIC, as shown in Figure 18a. Similarly, both oscillation and transient time in frequency deviation of the VSG were reduced by 50%, as shown in Figure 18b; this is translated as a reduction in the oscillation of the VSG output power, as shown in Figure 18c. The proposed controller was not only effective in quickly damping the oscillation and shortening the transient time of the VSG but also was able to do so with a significant reduction in the amplitude of the overshoot/undershoot of the output power. In other words, the proposed controller was able to combine the merits of the low inertia systems, which have short transient time, and the high inertia systems, which have lower

oscillation amplitude. The frequency–power angle trajectories and the resultant variation in the VSG inertia coefficient are shown in Figures 18d and 18e, respectively, which agree with the theoretical and mathematical model derived in the previous sections.

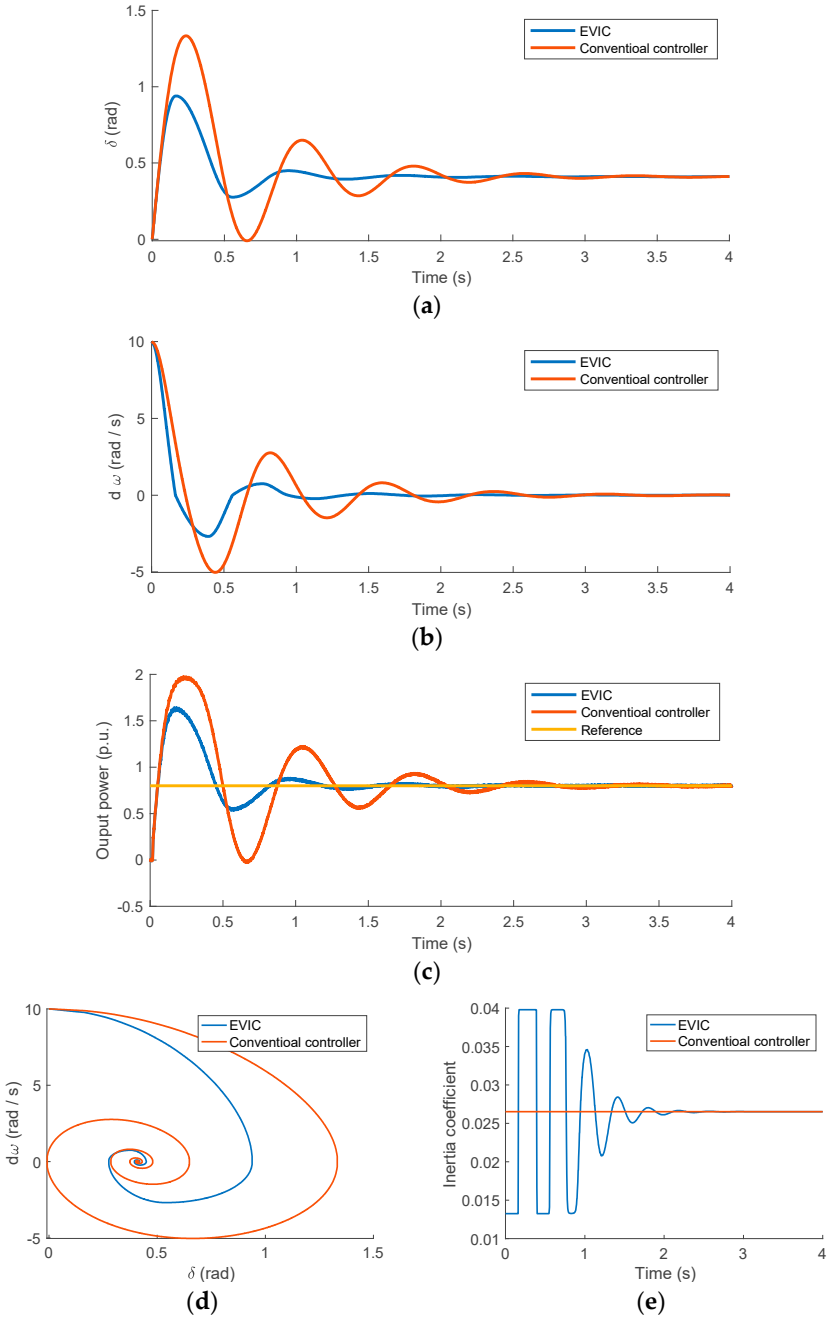


Figure 18. VSG converter performance under large disturbance, case I (orange is conventional inertia controller and blue is EVIC); (**a**) VSG power angle vs. time; (**b**) VSG frequency deviation vs. time; (**c**) VSG output power; (**d**) VSG power angle–frequency trajectory; and (**e**) VSG inertia coefficient.

The second case is considered to demonstrate the advantage of the proposed controller in increasing the VSG stability range in comparison with the conventional controllers. In this case, the initial power angle was set to $\delta_o = 0$ rad, and the frequency deviation from the infinite bus frequency was set to $\omega_o = 15$ rad/s. The results are shown in Figure 19. The conventional inertia controller was not able to bring the VSG back to stability, as clearly shown in its power angle and frequency, Figures 19a and 19b, respectively. On the other hand, the proposed controller, under the same conditions, was able to bring the VSG back

to its steady-state operating point δ_o without compromising either power oscillation or the transient time. The resultant output power in both cases is shown in Figure 19c. The frequency–power angle trajectories and the resultant variation in the VSG inertia coefficient are shown in Figures 19d and 19e, respectively. It is worth mentioning that for the proposed EVIC controller to maintain system stability, it had to aggressively change the inertial coefficient for a longer time between its maximum and minimum values before entering its linear region, as shown in Figure 19e.

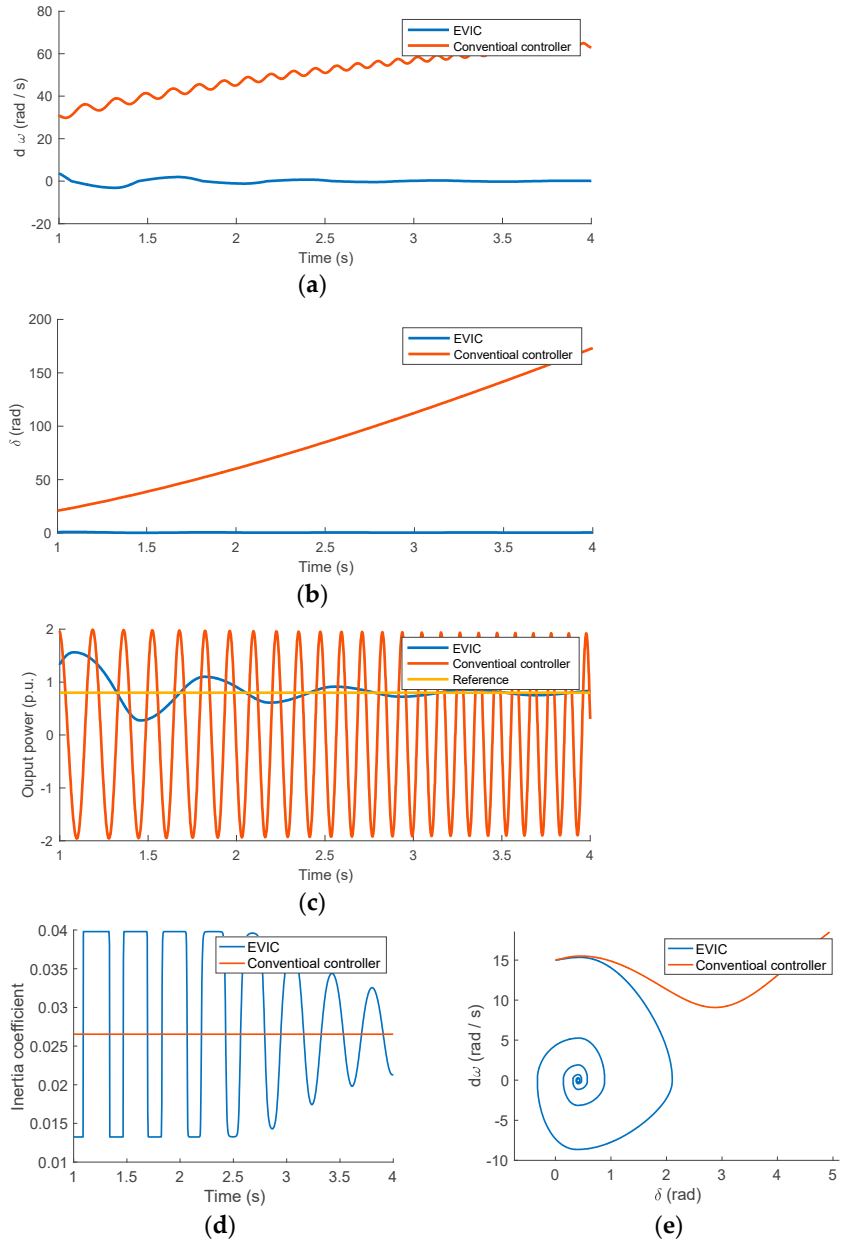


Figure 19. VSG converter performance under large disturbance, case II (orange is conventional inertia controller and blue is EVIC); (**a**) VSG power angle vs. time; (**b**) VSG frequency deviation vs. time; (**c**) VSG output power; (**d**) VSG power angle–frequency trajectory; and (**e**) VSG inertia coefficient.

Finally, the third case is when the VSG was subjected to a small load disturbance. Here, the power reference was increased by 1% from its original value of 0.8 p.u. The initial power angle was set at $\delta_o = 0.3908$ rad, and the frequency deviation from infinite bus frequency was set at $\omega_o = 0$ rad/s. The results shown in Figure 20a–e show that both the conventional inertia controller and the proposed controller perform identically when

being subjected to small amplitude disturbances. As discussed, this is an advantage of the proposed controller. That is, from a small signal point of view, the proposed controller has a well-defined inertia as opposed to other alternating inertia controller. Figure 20e shows a very small variation around the nominal inertia coefficient value, which is identical to its value in the conventional controller. Hence, it can be assumed constant in linearization; this means that all linearized models, analyses, and results are valid under the proposed controller, which saves time and effort that would have to be used to build other linear models and study their stability boundaries and so on.

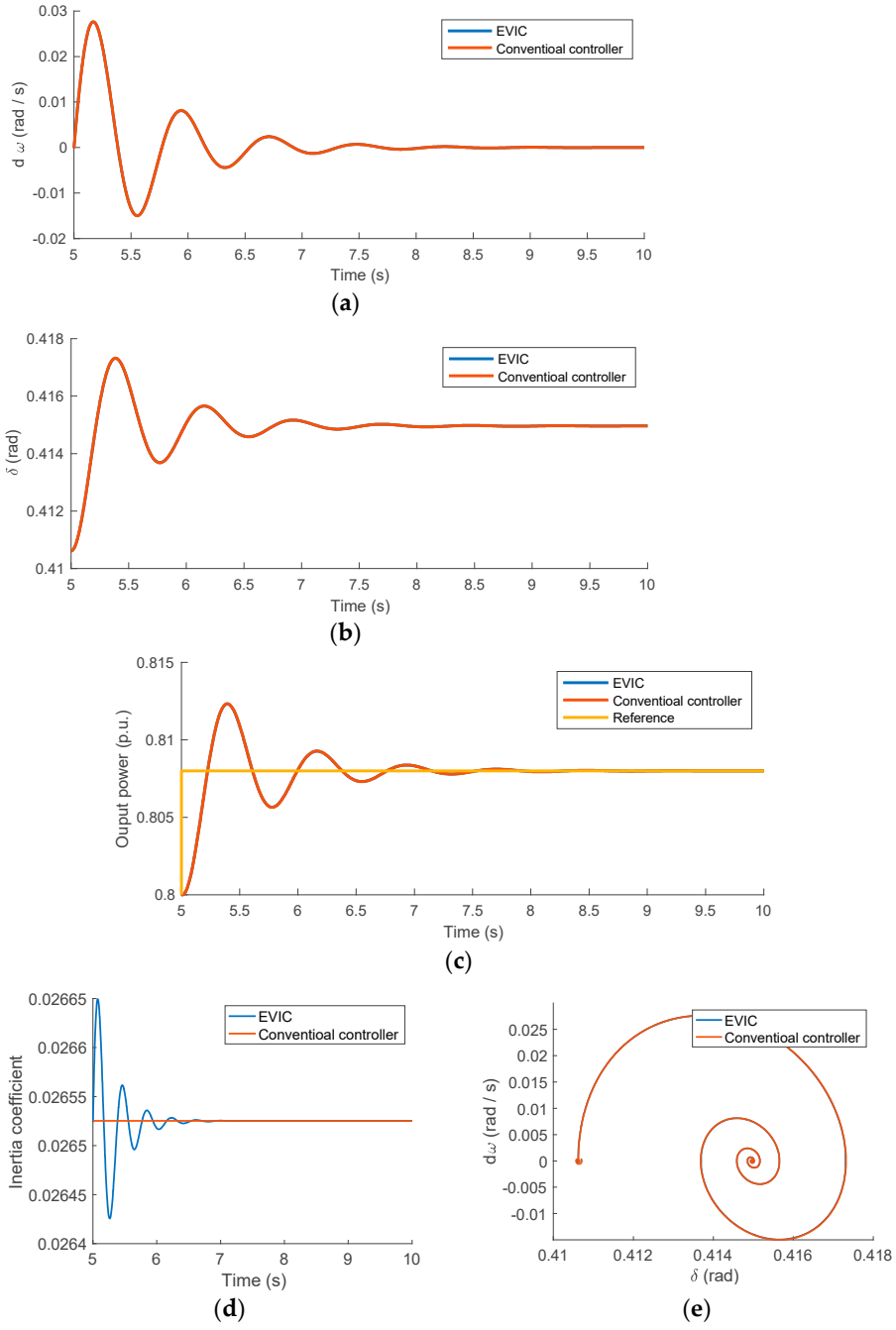


Figure 20. VSG converter performance under small disturbance, case III (orange is conventional inertia controller and blue is EVIC); (**a**) VSG power angle vs. time; (**b**) VSG frequency deviation vs. time; (**c**) VSG output power; (**d**) VSG power angle–frequency trajectory; and (**e**) VSG inertia coefficient.

6. Conclusions

A novel enhanced virtual inertia-controlled EVIC is proposed to increase MG stability. It adopts the alternating inertia control technique, which changes the converter's inertia between two levels to quickly damp frequency and power oscillations. The proposed EVIC improves on that concept by adding three different modes of inertia alternation. The first mode is equal to the converter nominal inertia defined by the desired system response to small disturbances. The second mode linearly varies the inertia coefficient of a given VSG in proportion to the amount of applied large disturbances. The third mode provides a hard switching between two levels of inertia to quickly bring the system closer to its stability point when VSG is subjected to very large disturbances. Moreover, the proposed control is implemented using a smooth continuous function, unlike other techniques which use discontinuous functions or complicated artificial intelligence algorithms; this is important when a system nonlinear stability study is performed. The results show the validity of the proposed controller in not only improving system dynamic responses but also increasing the MG's overall area of attraction and, hence, its stability boundaries. The results also showed that when the VSG is subjected to large disturbance, it was able to combine the merits of the low inertia systems, which have short transient time, and the high inertia systems, which have lower power and frequency oscillation amplitude. Moreover, the simulation results showed that the proposed controller improves the MG stability margin in terms of the system's region of attraction. Finally, the proposed controller model is valid under linearization, which facilitates the study of its stability using linear techniques.

Author Contributions: Methodology, A.S. and V.K.S.; Formal analysis, V.K.S.; Investigation, A.S.; Writing—review & editing, V.K.S. All authors have read and agreed to the published version of the manuscript.

Funding: This research was funded by [Natural Sciences and Engineering Research Council of Canada] grant number [RGPIN-2022-04011] and the APC was funded by [RGPIN-2022-04011].

Data Availability Statement: Not applicable.

Conflicts of Interest: The authors declare no conflict of interest.

References

1. Fang, J.; Tang, Y.; Li, H.; Li, X. A Battery/Ultracapacitor Hybrid Energy Storage System for Implementing the Power Management of Virtual Synchronous Generators. *IEEE Trans. Power Electron.* **2018**, *33*, 2820–2824. [CrossRef]
2. Saadatmand, S.; Shamsi, P.; Ferdowsi, M. Power and Frequency Regulation of Synchronverters Using a Model Free Neural Network-Based Predictive Controller. *IEEE Trans. Ind. Electron.* **2021**, *68*, 3662–3671. [CrossRef]
3. Cheng, H.; Shuai, Z.; Shen, C.; Liu, X.; Li, Z.; Shen, Z.J. Transient Angle Stability of Paralleled Synchronous and Virtual Synchronous Generators in Islanded Microgrids. *IEEE Trans. Power Electron.* **2020**, *35*, 8751–8765. [CrossRef]
4. Pan, D.; Wang, X.; Liu, F.; Shi, R. Transient Stability of Voltage-Source Converters with Grid-Forming Control: A Design-Oriented Study. *IEEE J. Emerg. Sel. Top. Power Electron.* **2020**, *8*, 1019–1033. [CrossRef]
5. Wang, W.; Jiang, L.; Cao, Y.; Li, Y. A Parameter Alternating VSG Controller of VSC-MTDC Systems for Low Frequency Oscillation Damping. *IEEE Trans. Power Syst.* **2020**, *35*, 4609–4621. [CrossRef]
6. Xiong, X.; Wu, C.; Hu, B.; Pan, D.; Blaabjerg, F. Transient Damping Method for Improving the Synchronization Stability of Virtual Synchronous Generators. *IEEE Trans. Power Electron.* **2021**, *36*, 7820–7831. [CrossRef]
7. Zhong, Q.-C.; Weiss, G. Synchronverters: Inverters That Mimic Synchronous Generators. *IEEE Trans. Ind. Electron.* **2011**, *58*, 1259–1267. [CrossRef]
8. Saadat, H. *Power System Analysis*, 3rd ed.; PSA Publishing: Alexandria, VA, USA, 2010.
9. Xiong, X.; Wu, C.; Blaabjerg, F.; Pan, D. An Improved Synchronization Stability Method of Virtual Synchronous Generators Based on Frequency Feedforward on Reactive Power Control Loop. *IEEE Trans. Power Electron.* **2021**, *36*, 9136–9148. [CrossRef]
10. Jongudomkarn, J.; Liu, J.; Yanagisawa, Y.; Bevrani, H.; Ise, T. Model Predictive Control for Indirect Boost Matrix Converter Based on Virtual Synchronous Generator. *IEEE Access* **2020**, *8*, 60364–60381. [CrossRef]
11. Wu, H.; Ruan, X.; Yang, D.; Chen, X.; Zhao, W.; Lv, Z.; Zhong, Q.-C. Small-Signal Modeling and Parameters Design for Virtual Synchronous Generators. *IEEE Trans. Ind. Electron.* **2016**, *63*, 4292–4303. [CrossRef]
12. Xu, Q.; Dragicevic, T.; Xie, L.; Blaabjerg, F. Artificial Intelligence-Based Control Design for Reliable Virtual Synchronous Generators. *IEEE Trans. Power Electron.* **2021**, *36*, 9453–9464. [CrossRef]

13. Andalib-Bin-Karim, C.; Liang, X.; Zhang, H. Fuzzy-Secondary-Controller-Based Virtual Synchronous Generator Control Scheme for Interfacing Inverters of Renewable Distributed Generation in Microgrids. *IEEE Trans. Ind. Appl.* **2018**, *54*, 1047–1061.
14. Liu, J.; Miura, Y.; Bevrani, H.; Ise, T. Enhanced Virtual Synchronous Generator Control for Parallel Inverters in Microgrids. *IEEE Trans. Smart Grid* **2017**, *8*, 2268–2277. [CrossRef]
15. Wang, F.; Zhang, L.; Feng, X.; Guo, H. An Adaptive Control Strategy for Virtual Synchronous Generator. *IEEE Trans. Ind. Appl.* **2018**, *54*, 5124–5133. [CrossRef]
16. Shintai, T.; Miura, Y.; Ise, T. Oscillation Damping of a Distributed Generator Using a Virtual Synchronous Generator. *IEEE Trans. Power Deliv.* **2014**, *29*, 668–676. [CrossRef]
17. Chamorro, H.R.; Torkzadeh, R.; Eliassi, M.; Betancourt-Paulino, P.; Rezkalla, M.; Gonzalez-Longatt, F.; Sood, V.K.; Martinez, W. Analysis of the Gradual Synthetic Inertia Control on Low-Inertia Power Systems. In Proceedings of the 2020 IEEE 29th International Symposium on Industrial Electronics (ISIE), Delft, The Netherlands, 17–19 June 2020; pp. 816–820.
18. Fang, J.; Li, H.; Tang, Y.; Blaabjerg, F. On the Inertia of Future More-Electronics Power Systems. *IEEE J. Emerg. Sel. Top. Power Electron.* **2019**, *7*, 2130–2146. [CrossRef]
19. Alipoor, J.; Miura, Y.; Ise, T. Power System Stabilization Using Virtual Synchronous Generator with Alternating Moment of Inertia. *IEEE J. Emerg. Sel. Top. Power Electron.* **2015**, *3*, 451–458. [CrossRef]
20. Mao, M.; Hu, J.; Ding, Y.; Chang, L. Multi-parameter Adaptive Power Allocation Strategy for Microgrid with Parallel PV/Battery-VSGs. In Proceedings of the 2019 IEEE Energy Conversion Congress and Exposition (ECCE), Baltimore, MA, USA, 29 September–3 October 2019; pp. 2105–2111.
21. Kerdphol, T.; Watanabe, M.; Hongesombut, K.; Mitani, Y. Self-Adaptive Virtual Inertia Control-Based Fuzzy Logic to Improve Frequency Stability of Microgrid with High Renewable Penetration. *IEEE Access* **2019**, *7*, 76071–76083. [CrossRef]
22. Chamorro, H.R.; Sevilla, F.R.S.; Rouzbehi, K.; Chavez, H.; Sood, V.K.; Gonzalez-Longatt, F. Innovative primary frequency control in low-inertia power systems based on wide-area RoCoF sharing. *IET Energy Syst. Integr.* **2020**, *2*, 151–160. [CrossRef]
23. D'arco, S.; Suul, J.A.; Fosso, O.B. A Virtual Synchronous Machine implementation for distributed control of power converters in SmartGrids. *Electr. Power Syst. Res.* **2015**, *122*, 180–197. [CrossRef]
24. Meng, J.; Wang, Y.; Fu, C.; Wang, H. Adaptive virtual inertia control of distributed generator for dynamic frequency support in microgrid. In Proceedings of the 2016 IEEE Energy Conversion Congress and Exposition (ECCE), Milwaukee, WI, USA, 18–22 September 2016; pp. 1–5.
25. Khalil, H. *Nonlinear Systems*, 3rd ed.; Pearson: Hoboken, NJ, USA, 2001.

Disclaimer/Publisher's Note: The statements, opinions and data contained in all publications are solely those of the individual author(s) and contributor(s) and not of MDPI and/or the editor(s). MDPI and/or the editor(s) disclaim responsibility for any injury to people or property resulting from any ideas, methods, instructions or products referred to in the content.